Ultrastructurally smooth thick partitioning and volume stitching for large-scale connectomics

Kenneth J Hayworth[1], C Shan Xu[1], Zhiyuan Lu[2], Graham W Knott[3], Richard D Fetter[1], Juan Carlos Tapia[4], Jeff W Lichtman[5] & Harald F Hess[1]

Focused-ion-beam scanning electron microscopy (FIB-SEM) has become an essential tool for studying neural tissue at resolutions below 10 nm × 10 nm × 10 nm, producing data sets optimized for automatic connectome tracing. We present a technical advance, ultrathick sectioning, which reliably subdivides embedded tissue samples into chunks (20 μm thick) optimally sized and mounted for efficient, parallel FIB-SEM imaging. These chunks are imaged separately and then 'volume stitched' back together, producing a final three-dimensional data set suitable for connectome tracing.

Today's scanning electron microscopes achieve ~2-nm spot diameters at landing energies low enough that only the top few nanometers of the block's surface contributes substantially to the acquired image. In FIB-SEM[1,2], this is combined with the ion beam's ability to polish (mill) away a few nanometers at a time. Repeating this cycle produces a sequence of images representing three-dimensional (3D) ultrastructure and gives this technique a 'section' (z) resolution significantly better[3] than those of serial-section techniques (for example, serial-section TEM[4,5] and automated tape-collecting ultramicrotome SEM[6]) and serial block electron microscopy[7].

Physically cutting ultrathin sections requires a knife sharpened (and positioned in height relative to the surface) to much less than the section thickness. In contrast, because ion milling is akin to sandblasting, FIB can be considered a 'soft knife' whose diameter can be over 100 times the desired surface-removal thickness. The beam's positioning accuracy is similarly less constrained and can be held constant relative to the surface simply by adjusting deflection voltages. In our lab, we have designed custom FIB-SEM microscopes taking advantage of these characteristics, allowing us to operate our FIB-SEM microscopes mostly unattended for months at a time.

However, the FIB-SEM technique has an Achilles' heel: ion polishing accumulates artifacts when milling blocks longer than a few tens of micrometers in the direction of the ion beam. Artifacts take the form of streaks and waves of thickness variation. In our hands, imaging regions longer than ~100 μm results in unacceptable artifacts, thus representing a fundamental barrier to applying FIB-SEM to the field of connectomics[8,9]. To overcome this barrier, we aimed to divide tissue into smaller chunks (**Fig. 1a**) that were each large enough to be cut and handled reliably but small enough for FIB-SEM. Such subdivision must be virtually lossless for the imaged chunks to be stitched back together into a single data set. We refer to such sections as ultrathick. An ultrathick series contains sections that are typically 20 μm or thicker. They are efficiently loadable into FIB-SEM microscopes (or serial block electron microscopes), and their surfaces are cut so cleanly that ultrastructural details remain traceable across the cuts.

We tested several techniques to obtain ultrathick sections. We first tried vibratomy of unembedded tissue, but this resulted in unacceptable damage to the cut surfaces. For ultrathin sectioning, this damage is avoided by infiltrating tissue with hard resin[10] to hold the ultrastructure in place. However, a hard block cut at 20 μm results in sections that crumble. As long ago as 1967, McGee-Russell and Gosztonyi[11,12] and, separately, West[13] developed a solution. Superficially heating the block's surface softens it locally, making it possible to cut sections thicker than 10 μm. These researchers showed that such sections can be resectioned for serial electron microscopy; however, they did not address surface damage, which, because they used metal blades, was likely considerable.

To assess what quality of surface could be obtained if 'hot-knife microtomy' was upgraded with a diamond knife, we built a knife heater and cut 20- to 30-μm sections. We found a temperature of 60 °C to be optimal. At colder temperatures, curling occurred; at higher temperatures, sections became distorted. However, SEM images of cut faces showed considerable damage, as water, which provides lubrication in traditional ultrathin sectioning, was ineffective for thick sectioning (**Supplementary Fig. 1**). Using oil for knife lubrication dramatically reduced stick-slip (the periodic sticking of the section on the knife surface during cutting) but did not eliminate it. As ultrasonic vibration has been shown to reduce compression[14] and may help maintain lubrication, we switched to using a heated ultrasonic knife. This eliminated stick-slip and distortions. We acquired SEM images of the surfaces of two matched 20-μm-thick sections (**Supplementary Figs. 2** and **3**). None of the previous damage was visible, and matching neuronal

[1]Janelia Research Campus, Howard Hughes Medical Institute, Ashburn, Virginia, USA. [2]Department of Psychology, Dalhousie University, Halifax, Nova Scotia, Canada. [3]Ecole Polytechnique Fédérale de Lausanne, Lausanne, Switzerland. [4]Department of Neuroscience, Columbia University Medical Center, New York, New York, USA. [5]Department of Molecular and Cell Biology, Harvard University, Cambridge, Massachusetts, USA. Correspondence should be addressed to K.J.H. (hayworthk@janelia.hhmi.org).

RECEIVED 11 AUGUST 2014; ACCEPTED 31 DECEMBER 2014; PUBLISHED ONLINE 16 FEBRUARY 2015; DOI:10.1038/NMETH.3292

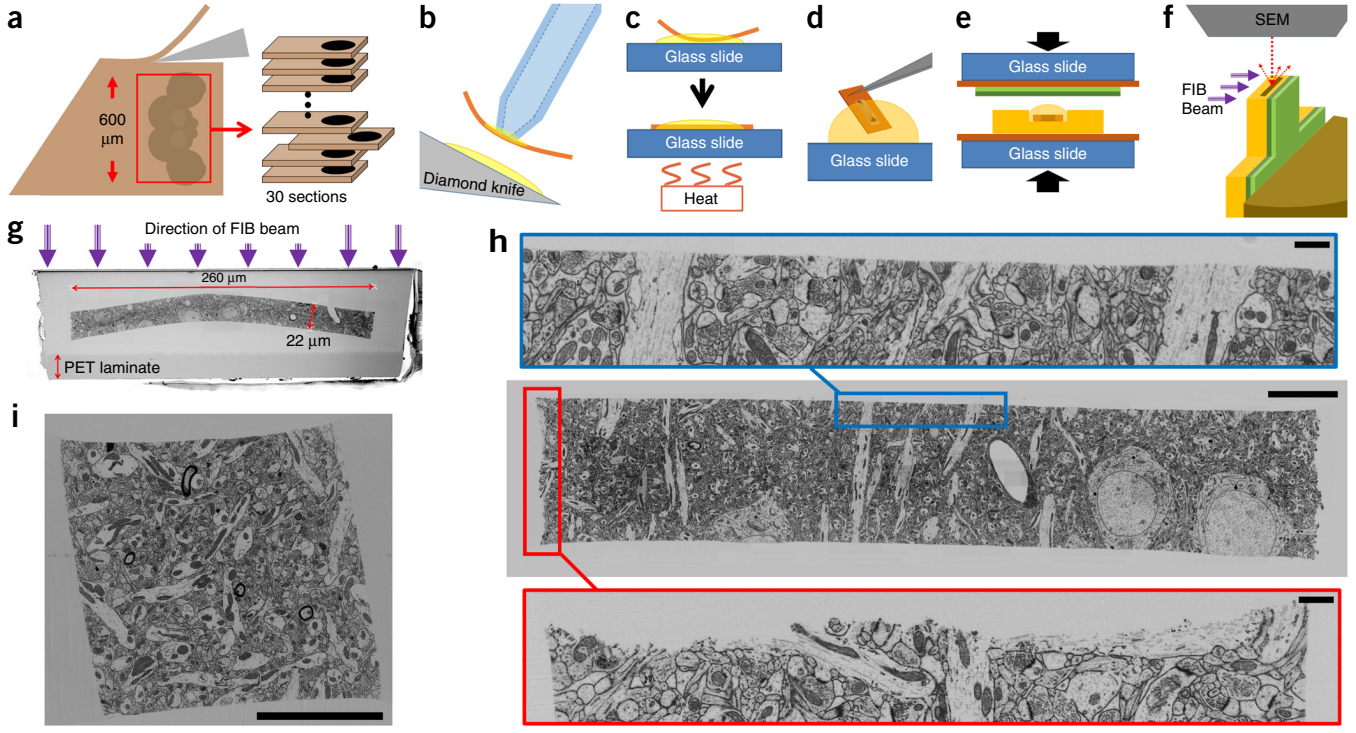

Figure 1 | Overview of ultrathick sectioning. (**a**) Tissue volumes with dimensions too large for FIB-SEM, such as an entire adult *Drosophila* brain, can be sectioned into optimally sized 'ultrathick' chunks and imaged across multiple FIB-SEM microscopes. (**b**–**f**) Steps involved in preparing ultrathick sections for FIB-SEM imaging. Oil-covered sections are retrieved using vacuum tweezers (**b**) and flattened with a hot plate (**c**). Oil is removed by dipping each section in a succession of Durcupan drops (**d**). Sections are flat embedded in Durcupan against a poly(ethylene terephthalate) (PET) laminate (green layers) (**e**). Sections are cut out and adhered to metal studs. Each tab is trimmed with a UV laser and diamond knife and then conductively coated to ready it for FIB-SEM imaging (**f**). (**g**) SEM image of the top surface of a sample tab. (**h**) FIB-SEM image of a 20-µm ultrathick section of mouse cortex cut from an original 100-µm vibratome section. Scale bars, 10 µm (center) and 1 µm (top and bottom). Magnified images of a smooth hot-knife cut edge (blue) and original vibratome cut (red) are shown. (**i**) Two-dimensional ultrathick sectioning. A 20-µm ultrathick section of mouse cortex was re-embedded and sliced orthogonally to the original cut plane, creating a square cross-section. Scale bar, 10 µm.

processes were readily traced across the cut faces. We built a custom ultrathick-sectioning test bed to include the ability to record top and side video microscope views and forces during sectioning (**Supplementary Fig. 4** and **Supplementary Video 1**).

Additional steps are required to prepare ultrathick sections for FIB-SEM imaging (**Fig. 1b**–**g**). We acquired 3D FIB-SEM stacks of ultrathick sections to evaluate cut quality (**Fig. 1h**,**i** and **Supplementary Videos 2** and **3**). We found that the cut surfaces were exceptionally smooth but not perfectly flat. Small undulations remained owing to local differences in rigidity. We developed algorithms to computationally flatten these surfaces so that sequential sections could be volume stitched (**Supplementary Figs. 5**–**7**). First, coordinates of the cut edge are found in each image individually, and then a 3D surface is fit representing the cut boundary. This is used to 'flatten' the edge in each image up to the same vertical position, resulting in a stack in which the cut surface resides in a single plane. The flattened surface images from two sequential ultrathick sections should match because they are two sides of the same physical cut. However, these images are expected to be distorted relative to one another owing to distortions during sectioning and embedding. We apply an image transformation that aligns one to the other. The two stacks can now simply be joined at their flattened surfaces, resulting in a final 3D volume ready for tracing.

To test the full procedure, we imaged with FIB-SEM and volume stitched two sequential 20-µm ultrathick sections, cut from a *Drosophila melanogaster* brain prepared via high-pressure freezing followed by freeze substitution (HPF-FS) (**Supplementary Fig. 8**). We imaged each section at a voxel size of 8 nm × 8 nm × 8 nm with a field of view encompassing the entire section (~120 µm × 32 µm) over a milling depth sufficient to encompass the entire lobula region (~80 µm). These large data sets (>1 terabyte) provided us the opportunity to survey thousands of square micrometers of matched cut area for significant damage. Because this volume of data overwhelms our current volume-stitching tools, the data set was collapsed to 32 nm × 32 nm × 32 nm voxels and then volume stitched (**Supplementary Videos 4** and **5**). A smaller data set was stitched at full resolution (**Supplementary Video 6**).

To test the procedure on mouse brain tissue, we imaged with FIB-SEM and volume stitched two sequential 20-µm ultrathick sections cut from a 100-µm-thick vibratome slice of mouse cortex (**Supplementary Fig. 9a**). Data sets were acquired (10 nm × 10 nm × 10 nm voxels) for matching edge regions of the two sections. We performed a volume stitch over a 9 µm × 16 µm cropped region (**Supplementary Fig. 9c**) and could easily identify matching neuronal processes across the stitch. This was verified by tracing 200 densely packed processes across the stitch (**Supplementary Fig. 9b** and **Supplementary Videos 7**–**9**).

Finally, we applied our procedure to tissue prepared by a different fixation procedure. We imaged with FIB-SEM and volume stitched two sequential 20-µm ultrathick sections cut from

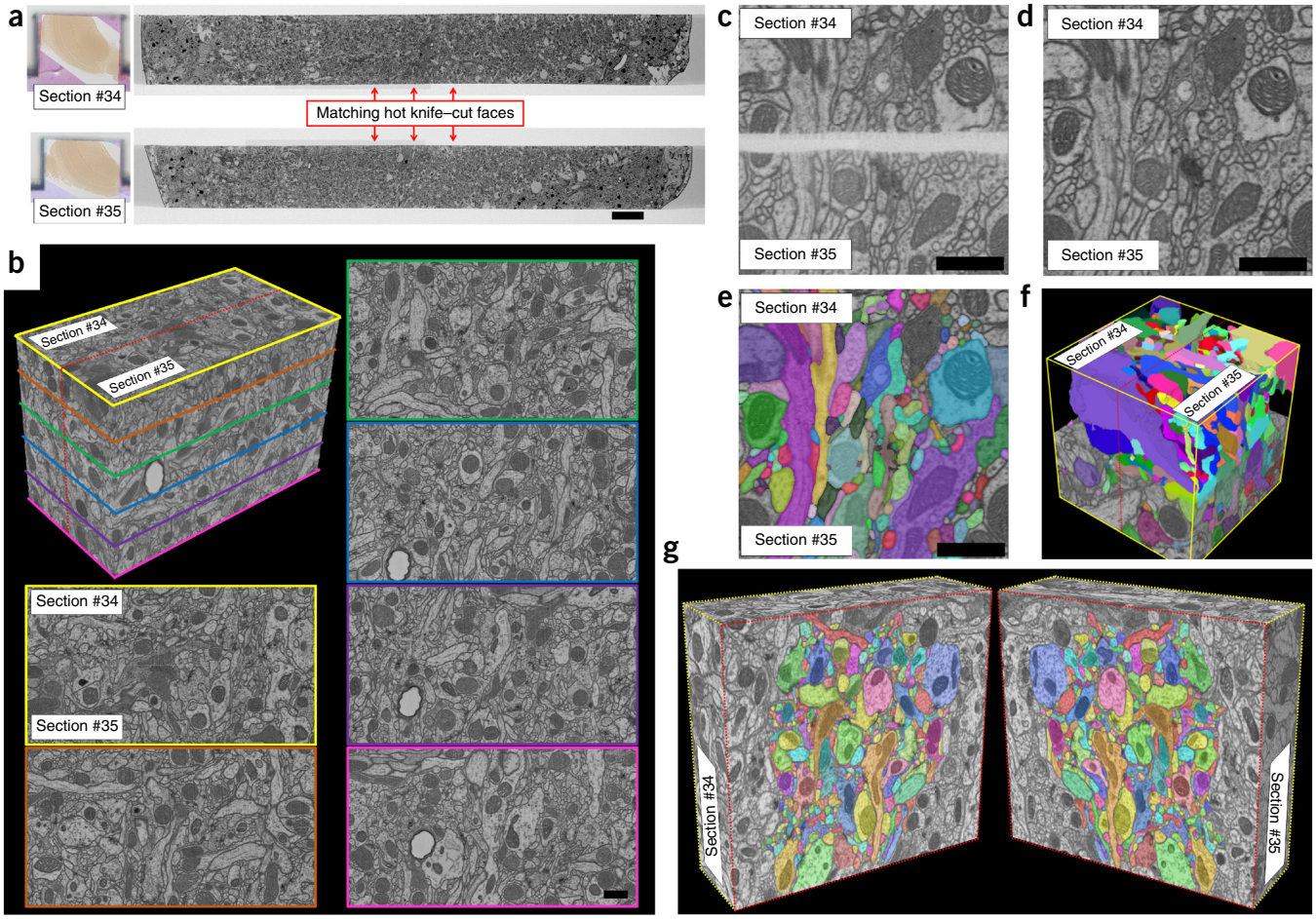

Figure 2 | Volume stitching on C-PLT–prepared *Drosophila* brain. (**a**) FIB-SEM images of two sequential 20-µm ultrathick sections. (**b**) Volume stitching over an 8 µm × 12 µm cropped region. The dotted red line on the 3D volume shows the stitch plane. Images with colored borders correspond to cut planes through this 3D stitched volume (**Supplementary Video 10**). (**c**,**d**) Aligned hot-knife cut edges before (**c**) and after (**d**) algorithmic flattening and stitching. (**e**,**f**) Volume tracing of the 4 µm × 4 µm × 4 µm volume from which **c**,**d** were obtained. **Supplementary Video 12** contains side-by-side movies of all slices of this same volume before and after stitching as well as after volume tracing. (**g**) 9 µm × 10 µm cropped region that has been split open along the stitch plane. Processes in the densely packed central region were traced across the gap (**Supplementary Video 11**). Scale bars, 10 µm (**a**) and 1 µm (**b**–**e**).

a *Drosophila* brain fixed chemically and processed using progressive lowering of temperature dehydration (C-PLT) (**Fig. 2a**). The C-PLT process provided high-contrast synaptic features (**Supplementary Fig. 10**). FIB-SEM data sets were acquired (8 nm × 8 nm × 8 nm voxels) for matching edge regions of the two sections. We performed a volume stitch over an 8 µm × 12 µm region (**Fig. 2b**–**f**). Matching neuronal processes were easily identified across the stitch. Processes in *Drosophila* reach smaller diameters than in mammalian cortex; therefore, we expected that tracing across the hot-knife stitch would be more difficult. We attempted to trace 406 densely packed processes across the stitch (**Fig. 2g**) and compared the results of two independent tracers. A total of eight processes were deemed to be sufficiently ambiguous to be considered untraceable by one or both tracers, implying a 98% traceability rate (**Supplementary Videos 10**–**12**).

Despite the fact that tracing was possible, some material had been lost between the two matching faces. This is most readily seen when the volume is digitally resliced parallel to the stitch. This material loss, combined with residual distortions due to imperfect alignment and ambiguities in the flattening algorithm, adds up to a 'jump' that appears visually similar to the loss of one traditional TEM section. By comparing the image correlation jump across the hot-knife stitch to virtual gaps of various amounts, we quantified this loss to be ~30 nm (**Supplementary Fig. 11**), which may affect the tracing of very small neurites (**Supplementary Figs. 12** and **13**).

Given an optimally prepared sample, the ultrathick sectioning process is very reliable. Because sections are so thick, even blocks larger than 1 mm^3 can be reduced to FIB-SEM tabs quickly. We have, however, run into some limitations with particular tissue samples (Online Methods). In general, tissue must be well fixed and infiltrated, but not overly brittle, for quality ultrathick sectioning.

The volume-stitched data sets presented demonstrate that it is possible to subdivide a block of brain tissue into smaller chunks optimally sized for efficient, artifact-free FIB-SEM imaging while retaining the ability to trace neuronal processes. This subdivision is not limited to one dimension. Re-embedding ultrathick sections and cutting them in an orthogonal direction can reduce a large block to square pillars or even cubes if desired (**Fig. 1i** and **Supplementary Fig. 14**). This opens up a range of possible connectomics studies by allowing FIB-SEM's excellent 3D resolution to be applied to arbitrarily large volumes of brain tissue.

METHODS

Methods and any associated references are available in the online version of the paper.

Note: Any Supplementary Information and Source Data files are available in the online version of the paper.

ACKNOWLEDGMENTS

We thank S. Takemura and S. Plaza for assistance with tracing, and R. Schalek for assistance with early electron microscopy imaging.

AUTHOR CONTRIBUTIONS

K.J.H. conceived of, designed and performed the experiments and wrote the manuscript. C.S.X., H.F.H. and K.J.H. constructed the custom FIB-SEM systems. C.S.X. designed and implemented the custom FIB-SEM control hardware and software. Z.L. developed the C-PLT technique and prepared the C-PLT tissue. G.W.K. prepared mouse cortex tissue for FIB-SEM (**Fig. 1** and **Supplementary Figs. 9** and **12**). J.C.T. prepared mouse tissue for earlier studies (**Supplementary Figs. 1**–**3** and **15**). R.D.F. prepared larva tissue. R.D.F. and Z.L. prepared HPF-FS tissue. Early research (**Supplementary Figs. 1**–**3**) was performed in the laboratory of J.W.L. All FIB-SEM research was performed in the laboratory of H.F.H.

COMPETING FINANCIAL INTERESTS

The authors declare no competing financial interests.

1. Knott, G., Marchman, H., Wall, D. & Lich, B. *J. Neurosci.* **28**, 2959–2964 (2008).
2. Xu, C.S. & Hess, H. *Microsc. Microanal.* **17**, 664–665 (2011).
3. Briggman, K.L. & Bock, D.D. *Curr. Opin. Neurobiol.* **22**, 154–161 (2012).
4. Harris, K.M. *et al. J. Neurosci.* **26**, 12101–12103 (2006).
5. Bock, D.D. *et al. Nature* **471**, 177–182 (2011).
6. Hayworth, K.J. *et al. Front. Neural Circuits* **8**, 68 (2014).
7. Denk, W. & Horstmann, H. *PLoS Biol.* **2**, e329 (2004).
8. Denk, W., Briggman, K.L. & Helmstaedter, M. *Nat. Rev. Neurosci.* **13**, 351–358 (2012).
9. Morgan, J.L. & Lichtman, J.W. *Nat. Methods* **10**, 494–500 (2013).
10. Hayat, M.A. *Principles and Techniques of Electron Microscopy* 4th edn. (Cambridge University Press, 2000).
11. McGee-Russell, S.M. & Gosztonyi, G. *Nature* **214**, 1204–1206 (1967).
12. McGee-Russell, S.M., De Bruijn, W.C. & Gosztonyi, G. *J. Neurocytol.* **19**, 655–661 (1990).
13. West, R.W. *Stain Technol.* **47**, 201–204 (1972).
14. Studer, D. & Gnaegi, H. *J. Microsc.* **197**, 94–100 (2000).

ONLINE METHODS

Sample preparation. *Drosophila* larva (**Supplementary Figs. 5a**,**b**, **6** and **7**): brains from wandering 3rd instar larvae of *[iso] Canton S G1 × w1118 [iso] 5905* flies were obtained by dissection from filleted preps on Sylgard (Dow Corning) plates in PBS and transferred to 2% glutaraldehyde in 0.1 M Na-cacodylate buffer, pH 7.4, fixative for 1 h at room temp. After being rinsed in 0.1 M Na-cacodylate buffer, the samples were post-fixed with 1% OsO4 in 0.1 M Na-cacodylate buffer, rinsed in buffer followed by distilled water and stained *en bloc* overnight with 1% aqueous uranyl acetate in a refrigerator. The samples were rinsed in water, dehydrated in an ethanol series followed by propylene oxide, and then infiltrated and embedded in Eponate 12 resin (Ted Pella).

Adult *Drosophila* brain prepared via HPF-FS fixation (**Supplementary Fig. 8**): high-pressure freezing followed by freeze substitution (HPF-FS) fly brain tissues were vibratome sliced (190 µm) from 5-d-old female adult Oregon R wild-type *Drosophila* heads. After 5 min of immersion in modified Karnovsky's fixative[15], the slices were cryofixed by a Wohlwend Compact 01 HPF machine and then processed in a Leica EM AFS2 freeze-substitution system. The tissues were warmed from −140 °C to −90 °C at 50 °C/h and freeze substituted in acetone-based cocktail (containing 1% osmium tetroxide, 0.1% uranyl acetate, 1% methanol and 5% water) at −90 °C for 36 h. Up to 5% water was added to enhance membrane contrast[16]. Next, the tissues were warmed up to −20 °C at 2 °C/h and kept at −20 °C for 26 h and then brought to 0 °C at 4 °C/h. Following FS, tissues were rinsed in pure acetone, infiltrated and embedded in Poly/Bed 812 (Luft formulations).

Mouse cortex (**Fig. 1g–i** and **Supplementary Fig. 9**): all experimental protocols were conducted according to US National Institutes of Health guidelines for animal research and were approved by the Institutional Animal Care and Use Committee at Janelia Research Campus. A male, adult (3-month-old) C57/bl6 mouse was deeply anesthetized with an intraperitoneal injection of sodium pentobarbitone (30 mg per kg body weight) and immediately perfused with glutaraldehyde (2.5%) and paraformaldehyde (2%) in phosphate buffer (0.1 M, pH 7.4). After 2 h at room temperature, the brain was removed and mounted in 4% agarose, and coronal slices were cut through the cortex with a vibratome (Leica Microsystems VT1200). The slices were washed in cacodylate buffer (0.1M), post-fixed with 1.5% potassium ferrocyanide and 1% osmium tetroxide (1 h), then with 1% osmium tetroxide alone (1 h) and finally in 1% aqueous uranyl acetate (1 h). After being washed in double-distilled water, they were dehydrated with increasing concentrations of ethanol, embedded in Durcupan resin, and hardened at 65 °C for 24 h, sandwiched between glass microscope slides.

Adult *Drosophila* brain prepared via C-PLT fixation (**Fig. 2**): chemical fixation and progressive lowering of temperature dehydration (C-PLT) is a modified conventional chemical fixation method. Good tissue preservation and enhanced contrast were achieved (**Supplementary Fig. 10**). Five-day-old adult female Canton S wild-type flies of *Drosophila* were used in this experiment. Isolated brain tissues were prefixed in 2.5% formaldehyde and 2.5% glutaraldehyde in 0.1 M phosphate buffer at pH 7.4 for 2 h at 22 °C. After washing, the tissues were post-fixed in 0.5% osmium tetroxide in ddH_2O for 20 min at 4 °C. After washing and *en bloc* staining with 1% aqueous uranyl acetate for 30 min, the PLT procedure started from 0 °C when the tissues were transferred into 10% acetone. The temperature was progressively decreased to −25 °C while the acetone concentration was gradually increased to 97%. The tissue was fixed in 1% osmium tetroxide, 0.2% uranyl acetate in acetone for 42 h at −25 °C. After PLT dehydration/fixation, the temperature was increased to 22 °C, and tissues were rinsed in pure acetone, then infiltrated and embedded in Poly/Bed 812 (Luft formulation).

Ultrathick sectioning. Sample blocks targeted for ultrathick sectioning were first mounted in a standard ultramicrotome tissue chuck (Leica) and trimmed on an UltraCut E ultramicrotome (Reichert-Jung) using a straight-sided diamond ultratrim knife (Diatome). Blocks were trimmed to have a rectangular face approximately 1.5 mm wide and 3 mm long with the tissue centered in that face (**Supplementary Fig. 4b**). This was to provide a large enough section with ample blank regions for manipulation with vacuum tweezers and forceps. Three of the sides were trimmed straight into the block the full depth of the tissue (which could be >1 mm). The side of the block that would be the trailing edge during hot-knife sectioning was given a slope (~45°). If this was not done, we found that this trailing edge would bend out during hot-knife sectioning, leading to problems.

Sample blocks containing the larva and the adult HPF-FS *Drosophila* brain were ultrathick sectioned directly on the same UltraCut E using a 35°-wedge-angle ultrasonic diamond knife and heating jig (**Supplementary Fig. 2a**). This heating jig was machined of a single block of aluminum and fitted with a 120-V cartridge heater (CSH-1011001/120V, Omega) and a surface thermocouple (SA1XL-J-SRTC, Omega). These were wired to a benchtop PID temperature controller (CSC32, Omega). Because of heat loss, the knife temperature was always 10–20 °C lower than the set-point temperature of the heating jig; therefore, we always recorded the temperature of the knife itself by immersing the temperature probe of a digital multimeter (Fluke 179/EFSP) in the oil covering the knife.

Cutting parameters for the adult *Drosophila* brain prepared via HPF-FS (**Supplementary Fig. 8**): the ultrasonic knife was tuned to a side-to-side resonance at 31.8 kHz by monitoring the knife's side with the laser vibrometer (CLV-2534, Polytec). Velocity measurement of the vibrometer was used to calculate the side-to-side motion of the knife to be ~1 µm peak-to-peak. The knife boat was filled with oil (thread cutting oil, Master Plumber), and drops of oil were applied to the knife periodically to maintain lubrication on front and back surfaces of the knife. Cutting speed of the microtome was set to 0.1 mm/s. We always take test cuts from a block and adjust temperature of the knife as needed to produce smoothly flowing sections with minimal curl. The temperature needed can vary dramatically with the embedding medium. For this run a knife temperature of 54 °C was used. A total of 30 sections (each 20 µm thick) were cut, covering all fly tissue in the block. Each section was retrieved from the bottom of the knife boat using metal forceps (we had not yet introduced the vacuum tweezers retrieval method, which we now consider superior) and transferred to individual wells in a plastic well plate.

Following the trimming on the UltraCut E, sample blocks containing mouse cortex tissue (**Fig. 1g–i** and **Supplementary Fig. 9**) and the Adult *Drosophila* brain prepared via C-PLT fixation (**Fig. 2**) were transferred (still mounted in tissue chuck) to the ultrathick-sectioning test bed (**Supplementary Fig. 4**), which is

designed to accept the same sample chucks as standard ultramicrotomes. Sectioning on the test bed was done with a 25°-wedge-angle 'cryo' diamond knife (Diatome) (**Supplementary Fig. 4d**). A drop of oil was applied to the knife before cutting each section to maintain lubrication on front and back surfaces of the knife. **Supplementary Video 1** shows top and side video microscope views of the sectioning and collection process.

Cutting parameters for mouse cortical tissue (**Fig. 1g–i** and **Supplementary Fig. 9**): the ultrasonic knife was tuned to a side-to-side resonance at 29.7 kHz (~0.5-µm peak-to-peak motion). Cutting speed was 0.1 mm/s, and knife temperature was 60 °C. Sections were removed from the surface of the knife by vacuum tweezers. A total of 24 sections were cut (each 20 µm thick), 16 of which contained tissue, and collected in a plastic well plate.

Cutting parameters for adult *Drosophila* brain prepared via C-PLT (**Fig. 2**): the ultrasonic knife was tuned to a side-to-side resonance at 29.9 kHz (~0.5-µm peak-to-peak motion). Cutting speed was 0.1 mm/s, and knife temperature was 59 °C. Sections were retrieved by vacuum tweezers. A total of 39 sections were cut (each 20 µm thick), 26 of which contained tissue spanning the entire fly brain. These were collected in a plastic well plate.

Re-embedding and orthogonal 'pillar' cutting test (**Fig. 1i**): to test the idea of second-order subdivision (i.e., pillars and cubes; see **Supplementary Fig. 14**), we used two of the 20-µm ultrathick sections of Durcupan-embedded mouse cortical tissue cut in the same run as those used in **Supplementary Figure 9**. These sections were then cleaned of oil and re-embedded (separated by a blank Epon spacer) in a hole drilled into the top of a blank Epon block oriented such that subsequent sectioning of these re-embedded 20-µm ultrathick sections would occur in a plane orthogonal to their original sectioning plane. After curing, the block was trimmed, and another series of 20-µm ultrathick sections were cut from this new block. These new ultrathick sections contained little tissue pillars with square cross-sections 20 µm × 20 µm wide. These were prepared for FIB-SEM imaging by the method described in **Figure 1b–f** (and below) so that a pillar's four smooth hot knife–cut sides would all show up in a FIB-SEM cross-section. **Figure 1i** shows one image from a FIB-SEM–acquired stack of such a tissue pillar.

Known limitations. Samples prepared with the (R)OTO method[17] to enhance osmium concentration tend to crack during sectioning, presumably because the increased density of heavy metal makes them brittle. This is a significant limitation because such enhancement is often used in connectomics[18]. Also, a densely stained block may section fine at 20 µm but crack when cut thicker. We have experimented with post-staining of ultrathick sections using the hot ethanolic technique[19] and found that contrast can be significantly increased throughout the full depth (20 µm) of an otherwise lightly stained section (**Supplementary Fig. 15**). It is unclear, however, whether such post-staining can be used to increase contrast in tissue that has already been well prepared with a protocol designed for use with block-face imaging, such as in the mouse cortical tissue shown in **Figure 1g–i** and **Supplementary Figure 9**.

Fly samples prepared using HPF-FS tend to rip at epithelial sheath boundaries under the stress of sectioning, damaging nearby tissue.

The preferred resin for FIB-SEM imaging is Durcupan (as it dramatically reduces streak artifacts); however, we have found it comparatively difficult to cut (relative to Epon), so we typically have used Epon-embedded tissue for ultrathick sectioning tests. Because these Epon-infiltrated ultrathick sections are eventually flat embedded in Durcupan (**Fig. 1e**), streaking is minimized but not eliminated. When we must cut Durcupan-embedded tissue, our solution has been to re-embed the Durcupan-infiltrated tissue in surrounding Epon (tested in **Supplementary Fig. 9**) before hot-knife sectioning—thus providing improved rigidity during cutting. Because these sections are eventually flat embedded in Durcupan, the resulting FIB-SEM tabs present only Durcupan to the ion beam.

In general, tissue must be well fixed and infiltrated, but not overly brittle, for quality ultrathick sectioning.

Mounting for FIB-SEM imaging. The ultrathick sections collected in plastic well plates were covered in cutting oil and retained some curl following hot-knife sectioning. Under a dissection microscope, individual sections were transferred, using fine tipped forceps, to the surface of a glass slide. Care was taken to ensure that there was a layer of oil between the section and the glass slide. If necessary, more oil was added. The glass slide was then placed on the top of a hot plate set to 200 °C. As the slide heated, the ultrathick section flattened in just a few seconds. We waited 5–10 s after flattening and then removed the glass slide from the hot plate. Flattened sections from an entire run were arranged in order on the glass slide and then imaged with a light microscope for later reference.

Removing the cutting oil from sections was done just before flat embedding. Uncured Durcupan resin (Durcupan ACM Epoxy Resin Kit (not water soluble), SPI supplies) was prepared (component formulation: A, 11.4 g; B, 10.0 g; C, 0.3 g; D, 0.05–0.10 g) and degassed under vacuum. Five large drops (several millimeters in diameter) of uncured Durcupan were placed on a glass slide under a dissection microscope. A flattened ultrathick section still covered with oil was grasped on a blank corner region with metal forceps and manually dipped repeatedly (about ten times) in the first Durcupan drop. Oil was seen to disperse into the uncured resin. The top and bottom surfaces of the section were then gently touched to a dry area of the glass slide to help remove excess resin before the section was dipped in the next drop. This process was repeated for all five resin drops, and then the section (now cleaned of oil) was placed in the groove of a 'groove mold' (previously cured out of Durcupan as well; see **Fig. 1e** and below) in which it would be flat embedded. This process was repeated for all sections of a run, with fresh Durcupan drops being prepared every three sections.

Sections from an entire run were flat embedded side-by-side in a precured Durcupan groove mold against a PET laminate. The objective was to ensure that, in the final FIB-SEM sample tabs, the embedded ultrathick sections were surrounded by a buffer zone of Durcupan on the side of the section facing the ion beam. This buffer zone acts like the front masking material (for example, platinum) used by other FIB-SEM researchers, helping to prevent milling streaks, and ensures that SEM images will include blank resin zones surrounding the embedded tissue. One way to ensure such a buffer zone is to precure a

doi:10.1038/nmeth.3292

flat block of blank Durcupan ~100 µm thick, having an ~50-µm-deep groove in it (see **Fig. 1e**).

Making of the groove mold: we have found that Kapton (polyimide) film provides excellent release properties for molding Durcupan. To make the groove mold, we first adhered a 25-mm-wide, 25-µm-thick strip of Kapton film (CS Hyde) to a glass slide, making the base of a mold-making mold that will be used to make the groove mold. We then cut 2-mm-wide strips of Kapton adhesive tape (silicone adhesive coated, CS Hyde) and stacked these to build up ~100-µm-tall walls on the base to serve as the sides of the mold-making mold. Then a ~50-µm-thick strip of adhesive Kapton tape was laid down the center of the base. This mold-making mold was then filled with Durcupan and flat pressed, in a clamp made from optical cage mounts (Thorlabs), against a top glass slide that was also covered with a strip of Kapton film. The clamp was placed in a 60-°C oven for 24–48 h to cure. One glass slide was removed and Kapton pieces were peeled away to expose the empty groove of the groove mold.

After being cleaned of oil, each section was placed in the bottom of the groove. As they were covered with uncured Durcupan resin, they were readily arranged and oriented as necessary by manipulation with forceps. Once all sections were placed in the groove, the groove was placed (with no top covering) in a 60-°C oven for ~2 h to partially cure and 'tack' the sections lightly in position in the groove. This prevents the sections from shifting and overlapping each other during final flat embedding. A 20-mm-wide, 25-µm-thick strip of PET film (PP24I, Polymex Clear one side heat sealable/one side untreated polyester film, Polyester Converter Ltd.) was then lightly adhered to a glass slide, acting as the top of the flat embedding clamp. The PET film was arranged so that its heat-sealable side was facing toward the tissue (resulting in a strong bond). The groove was filled with fresh Durcupan, and the arrangement was clamped (**Fig. 1e**) and put in a 60-°C oven for curing for 48 h.

After curing, the flat embedding clamp was removed and Kapton release film was peeled away, revealing a sturdy slab containing an entire run of ultrathick sections. Individual sections were cut out (using a scalpel), and the resulting tabs were adhered to custom metal studs using instant adhesive. A UV laser (LaserMill, New Wave Research) was used to trim each tab to the tissue dimensions. If no part of the tissue extended to the edge of the tab, then we would sometimes drill a small (40 µm × 40 µm) laser 'via' hole to expose part of the tissue to the surface of the tab. This was done to allow SEM imaging charges to drain away more effectively once the tab's surface was conductively coated. The sample tab was then mounted on an ultramicrotome, and its top surface only was trimmed using a diamond trimming knife (cryotrim20, Diatome). This trimming must be performed with the sample tab oriented so that its long direction is aligned with the cutting direction, otherwise the thin, high–aspect ratio tab will bend under the force of trimming. This susceptibility to bending is also why we trimmed the sides of tabs exclusively with the UV laser. Finally, 20 nm of gold followed by 100 nm of carbon was deposited on the sample while it was tilted and rotated in a vacuum coating machine (Model 682 PECS, Gatan). At this point the tabs were ready for standard FIB-SEM imaging.

FIB-SEM imaging. Sample tabs were imaged with FIB-SEM using either a Zeiss Sigma FE-SEM or a Zeiss Merlin FE-SEM. Both were fitted with Magnum FIB columns from FEI. Custom scan generation hardware and control software were used to coordinate the milling and imaging steps. (This software is not available as it is dependent on our custom hardware setup.)

Imaging parameters for adult *Drosophila* brain prepared via HPF-FS (optic medulla region, **Supplementary Fig. 8d–f**): Matching regions of the sample tabs containing ultrathick sections #17 and #18 were imaged with FIB-SEM in the Merlin FE-SEM using a 7-nA ion beam to mill away ~2-nm surface layers (25-s mill time) between each SEM image. SEM backscatter images were acquired with an 8-nA beam, 1.2-kV landing energy, 2.8-mm working distance, 8 nm × 8 nm pixel size, 0.25-µs dwell time. Raw images were aligned (SIFT align, FIJI[20]) and data collapsed to 8-nm isotropic voxels before volume stitching.

Imaging parameters for adult *Drosophila* brain prepared via HPF-FS (optic lobula region, **Supplementary Fig. 8b,c**): matching regions of the sample tabs containing ultrathick sections #17 and #18 were imaged with FIB-SEM in the Merlin FE-SEM using a 7-nA ion beam to mill away ~2-nm surface layers (25-s mill time) between each SEM image. SEM backscatter images were acquired with an 8-nA beam, 1.2-kV landing energy, 2.6-mm working distance, 8 nm × 8 nm pixel size, 0.25-µs dwell time. SEM images were taken with an ~120 µm × 32 µm field of view so that the entire ultrathick section was encompassed (**Supplementary Videos 2** and **3**). Both sections were imaged with FIB-SEM over an ~80-µm depth covering the full depth of the optic lobe's lobula region in each section. As a test of large-scale volume stitching, this data set was downsampled by taking every 16th image (i.e., spaced ~32-nm distances apart as milling thickness was ~2 nm per image), and these images were themselves scaled 0.25× in *x*, *y* (from 8 nm × 8 nm to 32 nm × 32 nm). The resulting images were then aligned (SIFT alignment, FIJI) into a 32 nm × 32 nm × 32 nm voxel data set suitable for testing volume stitching with our current software (**Supplementary Videos 4** and **5**).

Imaging parameters for mouse cortex (**Supplementary Fig. 9**): matching regions of the sample tabs containing ultrathick sections #21 and #22 were imaged with FIB-SEM in the Sigma FE-SEM using a 7-nA ion beam to mill away ~3-nm surface layers (20-s mill time) between each SEM image. SEM backscatter images were acquired with a 2-nA beam, 1.2-kV landing energy, 2.9-mm working distance, 5 nm × 5 nm pixel size, 0.8-µs dwell time. Raw images were aligned (SIFT align, FIJI) and data collapsed to 10-nm isotropic voxels before volume stitching.

Imaging parameters for adult *Drosophila* brain prepared via C-PLT fixation (**Fig. 2**): matching regions of the sample tabs containing ultrathick sections #34 and #35 were imaged with FIB-SEM in the Sigma FE-SEM using a 7-nA ion beam to mill away ~2-nm surface layers (30-s mill time) between each SEM image. SEM backscatter images were acquired with a 2-nA beam, 1.2-kV landing energy, 2.6-mm working distance, 8 nm × 8 nm pixel size, 0.8-µs dwell time. Raw images were aligned (SIFT align, FIJI) and data collapsed to 8-nm isotropic voxels before volume stitching.

Volume stitching. Our methodology for volume stitching is diagrammed in **Supplementary Figure 5c**. This process is broken into two main steps: (i) flattening each stack separately so that their hot knife–cut surfaces reside in a single plane and (ii) transforming one stack so that it aligns with the other stack,

thus allowing the two to be joined together across their flattened cut surfaces into a single 3D volume. We have written custom Matlab programs to perform each of these steps.

Flattening. We have written a custom GUI-based Matlab program (**Supplementary Software**) in which the user opens up a FIB-SEM stack containing a hot knife–cut edge in cross-section. The GUI allows the user to interactively test different image filtering and thresholding parameters, which are used by the algorithm for edge finding. The GUI also allows the user to graphically designate areas of the stack images that the edge-finding algorithm should ignore and, instead, simply extrapolate over on the basis of neighboring regions. This is required to prevent dirt particles (which sometimes are found clinging to the cut edge of the section) from causing deviations from the true cut edge. It is also required so that 'empty' biological features such as the *Drosophila* trachea air tubes (shown in **Supplementary Fig. 5** step #1 images) and the blood vessels in cortex are not treated as true edges by the algorithm. A user opens up a FIB-SEM stack in the program and scrolls through the stack designating with mouse drags and clicks the areas to be ignored and extrapolated over. Then the user uses a scroll bar to adjust a grayscale threshold used to optimally separate the tissue of the ultrathick section from the blank resin it is embedded in. Once set, the program automatically finds the image coordinates of the hot knife–cut edge in all stack images. It does this by first applying an anisotropic low-pass spatial filter (approximately aligned parallel to the edge) to the image and then walking along each pixel column from the blank resin region toward the tissue, looking for the first row position in which the pixel's grayscale value is below threshold (i.e., the first pixel containing tissue). Pixels at the physical cut boundary that contain stained membranes are easily found by this algorithm, but pixels at the physical cut boundary that contain lightly stained cytoplasm are often bypassed, resulting in the found edge containing many erroneous invaginations (see **Supplementary Fig. 6**). A smoothed curve is fit to this approximate edge, and all edge positions that deviate substantially from this smoothed curve are deleted. This subset of points is then used to fit another smoothed curve, and this process is iterated (three times) to get a final smoothed curve that best approximates the edge in that image. This process is done for all images in the stack separately; however, the previous image's found edge position is used to set the range over which the next stack's image is searched.

Once this process is completed, the program uses all of the found edges to fit a smoothed 3D surface approximating the full hot knife–cut boundary of this ultrathick section across the FIB-SEM stack. The program's GUI can be used to display, in different colors overlaid on the currently viewed FIB-SEM stack image, the initial approximate edge, the smoothed edge based on this stack image and the final smoothed edge based on the 3D smoothed surface, giving the user the ability to adjust parameters if necessary.

Once satisfied with the found edge, the user presses a button to direct the entire stack to be flattened. This is done by shifting columns of pixels in each image so that all of their found-edge pixels now reside in a single plane in the 3D flattened stack (see **Supplementary Fig. 5**).

Transforming and stitching. Once both the 'top' and 'bottom' stacks are flattened, we digitally reslice each stack (using FIJI) to make its flattened hot knife–cut surface parallel to the stack's image plane. (Note, this cut surface does not actually reside in a single image plane of this digitally resliced stack, but it is actually spread across about three image planes that are noisier and of lower contrast than other parts of the stack. This is due to loss of staining at the very surface of the cut as well as the approximate nature of the edge detection algorithm.) These digitally resliced stacks are then concatenated using FIJI, creating a single stack containing tissue on both sides of the hot-knife cut. However, in this combined stack, there are still many images containing blank resin separating the two sides of the tissue, and both sides are not aligned to each other.

This stack is then processed with the help of a custom Matlab script (**Supplementary Software**) that displays the top stack's surface image and the bottom stack's surface image side by side in Matlab's cpselect() alignment tool. This allows the user to choose corresponding landmarks in both images. For the volume-stitched stacks presented in this paper, the user selected ~100–200 points of correspondence spread across the surfaces. Once selected, these correspondence points are used by our program to define an image transformation that is applied to all of the digitally resliced images in the bottom stack using the Matlab function cp2tform(). (The type of image transformation used for **Supplementary Fig. 8d–f** and **Fig. 2** was pure affine, whereas cp2tform's "local weighted mean" transform was used for **Supplementary Figs. 8c** and **9**.) This process creates a new combined stack where the tissues on both sides of the cut are aligned with each other, but they are still separated by blank resin frames. The user simply removes these blank resin frames, and any frames containing some surface voxels but that are overall too noisy or low contrast to be gainfully included, from the stack. The result is the final volume-stitched stack, which is digitally resliced again to put it back into the same plane as the original FIB-SEM images (**Supplementary Fig. 5**).

Note that the stitch line in **Figure 2b**,**d** is harder to see than in **Supplementary Figure 9c**. This is because we digitally resliced the **Figure 2** volume parallel to the stitch plane and contrast-adjusted all images to have same grayscale mean and s.d. This compensated for a loss of stain contrast (described above) at the surface of the hot-knife cut (**Supplementary Video 10**).

Neurite tracing. In order to verify that processes could be traced across the stitch, we digitally resliced volume-stitched stacks (so that the stitch plane was parallel to the image plane) and loaded them into TrakEM2 (ref. 21). We endeavored to trace all processes crossing the stitch plane within a given area. For tracing of the cortical sample shown in **Supplementary Figure 9b**, we decided to trace 200 total processes, densely tracing until we reached that number. For tracing the C-PLT *Drosophila* sample shown in **Figure 2g**, we decided to trace 400 processes. Using TrakEM2's AreaLists, we manually colored only the profiles on image planes 2, 3 and 4 pixels from the stitch plane on both sides of the stitch; however, context information was used over planes further from the stitch plane as well. Processes where any ambiguity existed were examined by reslicing the isotropic stack in a different plane. As described in the text, <2% of processes crossing the stitch (in the C-PLT fly tissue) were sufficiently ambiguous to be considered untraceable by one or both of the two independent tracers. The TrakEM2 colored stacks are viewable online in **Supplementary Videos 9** and **11**.

doi:10.1038/nmeth.3292

We also performed volume tracing across the hot-knife stitch in the 4 μm × 4 μm × 4 μm volume shown in **Figure 2c–f** and in **Supplementary Video 12**. This volume tracing was performed by loading the stitched volume into the ilastik 1.1 software[22].

Red-green overlays and image mismatch comparisons. To generate the red-green overlay images shown in **Supplementary Figure 11**, the volume-stitched stack was first digitally resliced so that the stitch plane was parallel to the image plane of the stack. Then the stack's images were collapsed to faux 40-nm slices by averaging neighboring stack images and making sure not to average across the stitch plane itself. A control plane within this faux TEM stack was chosen at random, and that *N*th image was red-green overlaid with the $N + 1$ image to make the 0-nm gap overlay, with the $N + 2$ image to make the 40-nm gap and with the $N + 3$ image to make the 80-nm gap. The images on either side of the actual stitch plane were red-green overlaid to make the hot-knife overlay.

We used image correlation to help quantify our intuitive judgment that the hot knife–image jump was approximately equivalent to the 40-nm-gap's jump. For this, the images used for the red-green overlays were contrast inverted (to convert them back to signal levels) and filtered with a Gaussian filter of radius 4 (to remove noise that was clearly not relevant to the shift of membranes). The two images' grayscale values were then pixelwise subtracted, and the absolute values of these subtractions were averaged over all pixels to give a measure of image mismatch. For the cortical tissue of **Supplementary Figure 11a**, these image mismatches were: 0-nm gap = 3.1, 40-nm gap = 5.2, 80-nm gap = 6.3, hot-knife jump = 5.3. For the C-PLT *Drosophila* tissue of **Supplementary Fig. 11b**, these image mismatches were: 0-nm gap = 4.7, 40-nm gap = 6.8, 80-nm gap = 7.8, hot-knife jump = 6.4.

In **Supplementary Figure 11c**, we tried to quantify this hot-knife gap further for the C-PLT fly volume stitch. Four separate control planes within its faux TEM stack were chosen at random, and at each of these control planes the 0-nm-, 40-nm- and 80-nm-gap image mismatches were calculated as above. These image mismatches are plotted on the *y* axis of **Supplementary Figure 11c** versus nanometers removed on the *x* axis. Microsoft Excel was used to fit a second-order polynomial to these data, and this fit was used to determine the amount of nanometers removed that was equivalent to the observed hot knife–gap image mismatch (~30 nm).

15. Meinertzhagen, I.A. & O'Neil, S.D. *J. Comp. Neurol.* **305**, 232–263 (1991).
16. Walther, P. & Ziegler, A. *J. Microsc.* **208**, 3–10 (2002).
17. Seligman, A.M., Wasserkrug, H.L. & Hanker, J.S. *J. Cell Biol.* **30**, 424–432 (1966).
18. Tapia, J.C. *et al. Nat. Protoc.* **7**, 193–206 (2012).
19. Locke, M. & Krishnan, N. *J. Cell Biol.* **50**, 550–557 (1971).
20. Schindelin, J. *et al. Nat. Methods* **9**, 676–682 (2012).
21. Cardona, A. *et al. PLoS ONE* **7**, e38011 (2012).
22. Sommer, C., Strähle, C., Köthe, U. & Hamprecht, F.A. in *IEEE Int. Symp. Biomed. Imaging* 230–233 (2011).